Chapter 5

Radiative transfer of Lyα *photons*

5.1 Introduction

In chapter 3 we described the importance and usefulness of Lyα emitters as tracers of the dark matter distribution, particularly in the high redshift Universe. This is mostly due to the prominent spectral feature at 1216Å (in the rest frame), which arises from the downward transition between the levels $n = 2$ and $n = 1$ of hydrogen atoms in the interstellar medium of galaxies. Several observational techniques have been developed to search for the Lyα line in galaxies, with narrow band surveys being the most successful and common choice (Hu et al., 1998; Kudritzki et al., 2000; Gawiser et al., 2007; Nilsson et al., 2007b; Gronwall et al., 2007; Ouchi et al., 2008). Magnification of Lyα emission by galaxy lensing has also helped to detect candidates for very high redshift Lyα emitters (e.g. Stark et al., 2007). Integral field units are also being used to construct large surveys of Lyα emitters (Blanc et al., 2007; Hill et al., 2008)

From a theoretical point of view, perhaps the main uncertainty when modelling Lyα emission is the assumption about the fraction of Lyα photons which escape from the galaxy, f_{esc}. Lyα photons are very vulnerable to even small amounts of dust, due to the many scatterings they undergo before escaping from an HI region. Furthermore, other factors also play an important role, such as the kinematics, composition, temperature and geometry of the interstellar medium. This makes the modelling of the escape of Lyα photons a very challenging task.

There has been important progress over the last few years in modelling Lyα emitters in a cosmological setting. The first consistent hierarchical galaxy formation model which includes Lyα emission is the one described in Chapter 3 (see also Le Delliou et al., 2005, 2006; Orsi

et al., 2008), which makes use of the GALFORM semianalytical model. In this model, the simple assumption of a fixed escape fraction $f_{esc} = 0.02$, regardless of any galaxy property, allowed us to predict remarkably well the abundances and clustering of Lyα emitters in a wide range of redshifts and luminosities.

Kobayashi et al. (2007, 2010) attempted to include an empirical model of the escape of Lyα emitters in a different semianalytical model, predicting the correct abundances, UV luminosities and EWs of Lyα emitters. Nagamine et al. (2006, 2008) modelled Lyα emitters in cosmological SPH simulations, introducing a tunable escape fraction and duty cycle or stochasticity parameter $C_{Ly\alpha}$ (Lyα emission is assumed to *switch off* or be completely obscured in a random fraction of galaxies determined by $C_{Ly\alpha}$). Dayal et al. 2010a and Dayal et al. 2010b combined an SPH simulation with a radiative transfer model of ionizing photons to link the escape of continuum photons to the escape of Lyα at high redshifts. Their detailed modelling of the attenuation of the Lyα flux by the IGM allowed them to predict Lyα and UV luminosity functions in agreement with observations. However, a large degeneracy was found between the fraction of neutral hydrogen and the ratio of continuum to Lyα escape fractions assumed.

A more physical approach to modelling the escape of Lyα photons requires a treatment of the radiative transfer processes that photons undergo when travelling through an HI region. The scattering and destruction of Lyα photons have been extensively studied in the past, due to its many applications in astrophysical media. Due to the great complexity of the problem, numerical methods have been developed since the sixties to study specific problems, such as the mean number of scatterings a Lyα photon will experience before leaving a medium of a given optical depth, and the emerging flux from extremely thick media (Osterbrock, 1962; Avery and House, 1968; Adams, 1972).

Nowadays, numerical methods allow us to study the line profiles and escape fractions of Lyα photons in a variety of physical configurations. The standard method is to use a Monte Carlo algorithm, in which the path of a set of photons is followed one at a time through each scattering event, until the photon either escapes or is absorbed by a dust grain. These calculations have been succesfully applied to study the properties of Lyα emitters in different scenarios: Ahn 2003 (see also Ahn 2004) developed an outflow model to predict and

characterise the Lyα line profiles coming from starbursts at high redshifts. Verhamme et al. shown in a series of papers (Verhamme et al., 2006; Schaerer and Verhamme, 2008; Verhamme et al., 2008) that photons escaping from a spherically symmetric shell with a homogeneous hydrogen number density can reproduce the observed Lyα profiles of a sample of observed Lyman-break galaxies. Also Laursen et al. studied the variety of Lyα profiles and escape fractions obtained from a sample of galaxies taken from an SPH simulation (Laursen and Sommer-Larsen, 2007; Laursen et al., 2009a,b). Zheng and Miralda-Escudé 2002 (see also Dijkstra et al. 2006; Barnes and Haehnelt 2010) applied a Lyα radiative transfer code to study the properties of Damped Lyα Absorption systems (DLAs). Hansen and Oh (2006) used a similar code to study the effect of a multiphase medium (where dust is concentrated in clouds rather than being homogeneously distributed) on the emerging Lyα flux and escape fraction. Tasitsiomi (2006) applied their Lyα radiative transfer code to an SPH simulation to study the emergent Lyα flux of a $z \sim 8$ galaxy.

Despite this variety of theoretical work, there has not been any attempt to incorporate a detailed Lyα radiative transfer model in a fully fledged galaxy formation model. That is the goal of the next two chapters of this thesis: To develop a Lyα radiative transfer code in order to combine it with the GALFORM semi-analytical model to get an insight of the physical properties that affect the escape fraction of Lyα photons and the observed properties of Lyα emitters.

In the following, we will describe the physics and numerical implementation of the radiative transfer of Lyα photon when crossing a dusty HI region. The result of coupling this calculation to the GALFORM code will be discussed in the next chapter. The Monte Carlo radiative transfer code developed here is similar to other codes developed in the past, and mostly follows previous work by Zheng and Miralda-Escudé (2002); Verhamme et al. (2006); Dijkstra et al. (2006) and Laursen et al. (2009a).

5.2 Basics of Lyα radiative transfer

It is convenient to express frequencies, ν, in terms of

$$x \equiv \frac{(\nu - \nu_0)}{\Delta\nu_D}, \tag{5.1}$$

where $\Delta\nu_D = \nu_{\rm th}\nu_0/c$, c is the speed of light, and $\nu_{\rm th}$ is the thermal velocity of the hydrogen atoms in the gas, which is given by

$$\nu_{\rm th} = \left(\frac{2k_BT}{m_p}\right)^{1/2}, \tag{5.2}$$

where k_B is the Boltzmann constant, T is the gas temperature, m_p is the proton mass and ν_0 is the central frequency of the Lyα line, $\nu_0 = 2.47 \times 10^{15}$Hz.

When a Lyα photon interacts with an hydrogren atom, the scattering cross section, in the rest frame of the atom is given by

$$\sigma_\nu = f_{12}\frac{\pi e^2}{m_e c}\frac{\Gamma/4\pi^2}{(\nu-\nu_0)^2 + (\Gamma/4\pi)^2}, \tag{5.3}$$

where $f_{12} = 0.4162$ is the Lyα oscillator frequency, and $\Gamma = A_{12} = 6.25 \times 10^8 s^{-1}$ is the Einstein coefficient for the Lyα transition ($n = 2$ to $n = 1$).

The optical depth of a Lyα photon with frequency ν is determined by convolving this cross section with the velocity distribution of the gas,

$$\tau_\nu(s) = \int_0^s \int_{-\infty}^{+\infty} n(V_z)\sigma(\nu, V_z)\, {\rm d}V_z {\rm d}l, \tag{5.4}$$

where V_z denotes the velocity component along the photon's direction. Atoms are assumed to have a Maxwell-Boltzmann velocity distribution. In Doppler units, the optical depth can be written as

$$\tau_x(s) = \sigma_H(x) n_H s = 5.868 \times 10^{-14} T_4^{-1/2} N_H \frac{H(x,a)}{\sqrt{\pi}}, \tag{5.5}$$

where n_H is the hydrogen density, N_H the corresponding hydrogen column density, T_4 the temperature in units of 10^4K and a is the Voigt parameter, defined as

$$a = \frac{\Gamma/4\pi}{\Delta\nu_D} = 4.7 \times 10^{-4} T_4^{-1/2} \tag{5.6}$$

The Hjerting function $H(x,a)$ (Hjerting, 1938) describes the Voigt scattering profile,

$$H(x,a) = \frac{a}{\pi}\int_{-\infty}^{+\infty} \frac{e^{-y^2}\, {\rm d}y}{(y-x)^2 + a^2}, \tag{5.7}$$

which is often approximated by a central resonant core and power-law “damping wings" for frequencies below/above a certain boundary frequency x_c, which typically ranges between $2.5 < x_c < 4$. As a consequence, photons with frequencies close to the line centre have a large scattering cross section compared to those with frequencies in the wings of the profile. Hence, photons will be more likely to escape a medium when they have a frequency away from the line centre.

Scattering events are considered to be *coherent* (the frequency of the photon is the same before and after the scattering event) only in the rest frame of the atom, but not in the observer's frame. Thus, the thermal motion of the atom, plus any additional bulk motion of the gas, will potentially change the frequency of the photons, giving them the chance to escape from the resonant core. We will study this in detail in the next section.

5.3 A Monte Carlo radiative transfer code

Our goal is to understand the transfer of Lyα radiation in a large variety of physical configurations, so that we can apply our results to galaxies predicted by GALFORM. Of particular interest are the emergent spectrum of the Lyα line and the escape fraction of Lyα photons f_{esc}.

The above quantities have been computed analytically for some specific cases. Harrington (1973) computed the emergent spectrum of Lyα photons generated at the line centre escaping from an optically thick, static, homogeneous and dust-free infinite slab. Almost 20 years later, Neufeld (1990) generalised the previous result allowing the Lyα photons to be generated with frequencies away from the line centre. Later on, Dijkstra et al. (2006) followed a similar procedure to that of Harrington and Neufeld to compute the emergent spectrum from an optically thick, static, homogeneous, dust-free sphere.

As for the escape fraction in the presence of dust, less analytical progress has been made due to the complexity of the task. Neufeld (1990) computed the escape fraction of Lyα photons from an optically thick, static, homogeneous dusty slab. Using a Monte Carlo code, Hansen and Oh (2006) computed f_{esc} in a variety of multi-phase media, and provided fitting formulae based on the Neufeld expression for f_{esc}.

Evidently, the above results are not suitable to study more general cases, which is why we have developed our own Monte Carlo numerical code to compute the escape of Lyα photons in a wide variety of possible scenarios.

Monte Carlo radiative transfer codes work on a 3D grid in which each cell will contain information about the neutral hydrogen density n_H, the temperature of the gas T, the bulk velocity $v_{\rm bulk}$, and the probability of emitting a Lyα photon, which could, for instance, depend on the distribution of sources, for instance. Once a Lyα photon is created, a random direction and frequency are given to it, and the code must follow its trajectory and compute each scattering event of the photon until it either escapes or is absorbed by a dust grain. If the photon escapes, then its final frequency is recorded. In the following, we will call ξ_n a random number in the range $0 < \xi_n < 1$, where the subscript $n = 1, 2...$ reffers to different random numbers when more than one is used in a given calculation.

5.3.1 Initial direction and frequency

The initial direction of the photon is randomly selected using the transformations

$$\theta = \cos^{-1}(2\xi_1 - 1), \tag{5.8}$$

$$\phi = 2\pi\xi_2, \tag{5.9}$$

where ξ_1 and ξ_2 are two random numbers, and θ and ϕ are in radians. The initial frequency of the photon in the rest frame of the medium (which may not be static) will be, in Doppler units, $x_i' = 0$. In the observer's rest frame, the initial frequency of the photon will be

$$x_i = x_i' + \boldsymbol{n_i} \cdot \boldsymbol{v_{\rm bulk}}/v_{th}, \tag{5.10}$$

where $\boldsymbol{v_{\rm bulk}}$ is the bulk velocity vector of the gas at the location of the emission, and $\boldsymbol{n_i}$ is the direction of emission in cartesian coordinates, given by

$$\boldsymbol{n_i} = (\sin\theta\cos\phi, \sin\theta\sin\phi, \cos\theta) \tag{5.11}$$

5.3.2 Distance travelled

The location of the interaction (with either a dust grain or a hydrogen atom) is calculated as follows. The optical depth $\tau_{\rm int}$ the photon will travel is determined from the probability

distribution

$$P(\tau) = 1 - e^{-\tau}, \tag{5.12}$$

and so

$$\tau_{\rm int} = -\ln(1-\xi). \tag{5.13}$$

This optical depth corresponds to a distance travelled s given by

$$\tau(s) = \tau_x(s) + \tau_d(s), \tag{5.14}$$

where $\tau_x(s)$ and $\tau_d(s)$ are the optical depths due to hydrogen atoms and dust grains respectively. The length of the path travelled is determined by finding the distance s where $\tau(s) = \tau_{\rm int}$ by setting

$$s = \frac{\tau_{\rm int}}{n_H\sigma_x + n_d\sigma_d}, \tag{5.15}$$

where n_d and σ_d, the number density of dust grains and cross-section for interaction with dust, are described below.

The cross-section for scattering with a hydrogen atom depends on $H(x)$ (see Eq. 5.5), which looks like a Gaussian in the core and a power law in the wings:

$$H(x,a) \sim \begin{cases} e^{-x^2}, & \text{core} \\ \frac{a}{\sqrt{\pi}x^2}, & \text{wings.} \end{cases} \tag{5.16}$$

These two approximations break down in the transition domain, which is why we choose to compute the integral in Eq. (5.7) numerically and store the values of $H(x,a)$ in a table for a wide range of x and a. For frequencies larger than the one used to compute $H(x,a)$ numerically ($x_{max} = 500$), we use the power law approximation given in Eq. (5.16). This alternative both improves the performance (it is faster to compute the expression of (5.16) rather than interpolate values from a very long look-up table) and extends the validity of the code over a very wide range in x.

Sometimes the distance travelled makes the photon leave the cell from which it originated. In this case, the physical conditions can change, and, thus, this may affect the distance the photon was originally intended to travel. For instance, if the number density of hydrogen drops between two adjacent cells, then the total distance travelled by the photon will be larger than that originally computed, since the optical depth in the low density cell

translates into a larger travel distance than in the higher density cell. Temperature gradients and relative bulk motions between two adjacent cells have a similar effect on the total distance travelled. To overcome this problem, we compute how much optical depth is used after crossing each cell, until there is no more *available* optical depth to use. Numerically, when the distance computed is larger than the distance of the photon to the edge of the cell it is pointing to, then we let the photon travel to that edge, and compute the optical depth expended in this part of the motion. Then we recompute a new distance using the conditions in the new cell using Eq. (5.14), and repeat the procedure until all the original optical depth assigned to the photon according to Eq. (5.13) has been used.

The final location of the photon corresponds to the point where it interacts with either a hydrogen atom or a dust grain. To find out which type of interaction the photon experiences, we compute the probability $P_H(x)$ of being scattered by a hydrogen atom, given by

$$P_H(x) = \frac{n_H \sigma_H(x)}{n_H \sigma_H(x) + n_d \sigma_d}. \tag{5.17}$$

We generate a random number ξ and compare it to P_H. If $\xi < P_H$, then the photon interacts with the hydrogen atom, otherwise, it interacts with dust.

5.3.3 Dust scattering and absorption

Observationally, the extinction A_V is found to be proportional to the column density of hydrogen both within the Milky Way and in the Magellanic clouds (Massa and Fitzpatrick, 1986; Fitzpatrick and Massa, 2007), although with different proportionality coefficients.

Nevertheless, the cross section of dust interaction $\sigma_d(\lambda)$ can be expressed as an effective cross section per hydrogen atom. This eliminates any dependence of the cross section on the dust size distribution, grain shapes, etc, and relies merely on observed extinction curves. The optical depth of dust τ_d can be written as

$$\tau_d = \sigma_d N_d, \tag{5.18}$$

where σ_d is the cross section of dust particles (absorption plus scatterings), and N_d the column density of dust, $N_d \propto \Sigma_{\rm dust}$. On the other hand, the column density of hydrogen, $N_H \propto \Sigma_{\rm gas}$. To relate both we assume that the mass of dust can be related to the mass of the gas and the metallicity through

$$M_{\rm dust} = \epsilon M_{\rm gas} Z_{\rm gas}, \tag{5.19}$$

where $\epsilon = \delta_*/Z_*$, and δ_* is the dust-to-gas ratio at the solar metallicity $Z_* = 0.02$. We can write then

$$N_d \propto N_H Z_{\rm gas}, \tag{5.20}$$

which makes

$$\frac{\tau_d}{N_H} \propto Z_{\rm gas}. \tag{5.21}$$

The ratio τ_d/N_H can be obtained at solar metallicity from a tabulated extinction curve. If

$$\frac{\tau_d}{N_H}(Z_\odot) = E_\odot, \tag{5.22}$$

then we find

$$\tau_d = \frac{E_\odot}{Z_\odot} Z_{\rm gas} N_H. \tag{5.23}$$

Now, the optical depth of dust can be split in two separate terms, accounting for absorption and scatter by dust grains: $\tau_d = \tau_a + \tau_s$. Both are related by the albedo A, which is the probability of a photon being scattered when interacting with a dust grain. Thus, if A is known we have

$$\tau_a = (1-A)\frac{E_\odot}{Z_\odot} Z_{\rm gas} N_H. \tag{5.24}$$

Notice that τ_d and A are assumed not to depend on the photon frequency, since over the typical frequency range photons travel both quantities do not vary significantly, even if thermal motion of dust grains are considered.

When interacting with a dust grain, a Lyα photon can be either absorbed or scattered. This depends on the albedo of dust particles. At the wavelength of Lyα, the albedo is usually $A \sim 0.4$, depending on the extinction curve used. If the Lyα photon is absorbed, then it is lost forever. If not, then it will be scattered. The new direction will depend on a probability distribution for the elevation angle θ, whereas for the azimuthal angle ϕ the scattering will be symmetric. The scattering angle θ can be obtained from Henyey and Greenstein (1941) phase function

$$P_{HG}(\mu) = \frac{1}{2}\frac{1-g^2}{(1+g^2-2g\mu)^{3/2}}, \tag{5.25}$$

where $\mu = \cos\theta$ and $g = \langle\mu\rangle$ is the asymmetry parameter. If $g = 0$, Eq.(5.25) reduces to isotropic scattering. $g = 1(-1)$ implies complete forward (backward) scattering. In general g depends on the wavelength. For Lyα, $g = 0.73$.

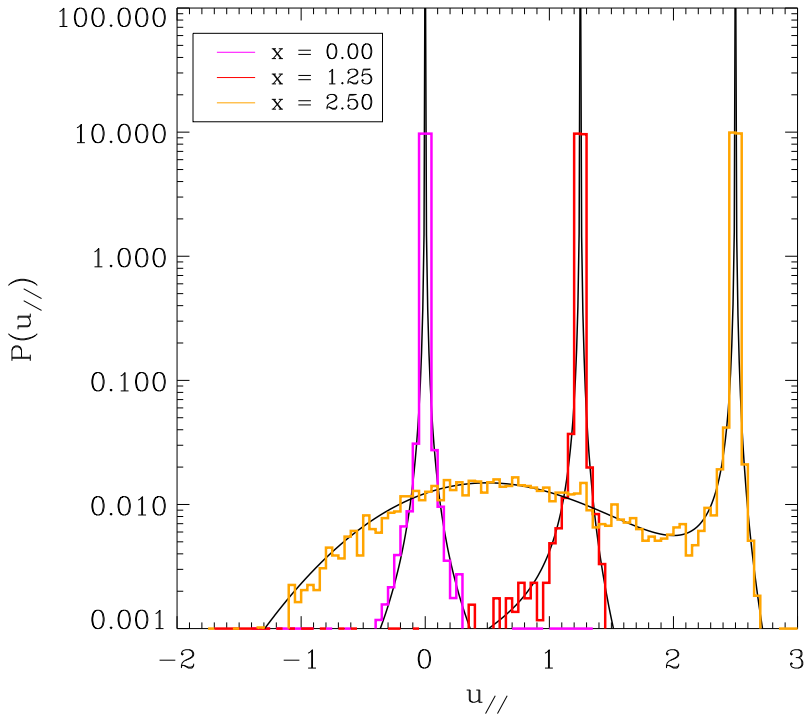

Figure 5.1: Probability distribution function of velocities of the scattering atom $u_{\parallel}$ parallel to the photon's direction for 3 values of the frequency of the incoming photon. The solid curves show the distribution from Eq. (5.27), and the histograms show the numerical results from the method described in section 5.3.4.

If the photon is interacting with dust, then we generate a random number ξ_1 to determine whether it is going to be absorbed or scattered, comparing this number to A. If the photon is absorbed, then it is lost. If it is scattered, then a new direction must be drawn.

5.3.4 Hydrogen scattering

Scattering by hydrogen atoms is more tricky. Inside an HI region, atoms move in random directions with velocities given by the Maxwell-Boltzmann distribution. Each of these atoms will *see* the same photon moving with a different frequency, due to the Doppler shift caused by their velocities. Since the cross section for scattering depends on the frequency of the photon, the probability for an atom to interact with a photon will depend on a combination of the frequency of the photon and the velocity of the atom.

The total velocity of the atom, $\boldsymbol{v}$, that scatters the Lyα photon, is given by the sum of the

bulk velocity of the gas plus the thermal velocity

$$\boldsymbol{v} = \boldsymbol{v}_{\rm bulk} + \boldsymbol{v}_{th}. \tag{5.26}$$

In the directions perpendicular to the photon's direction, $\boldsymbol{n_i}$, the two perpendicular components of the velocity of the atom $v_{\perp,1,2}$ follow a Gaussian distribution. The velocity component parallel to the photon's direction, $v_{\parallel}$, will depend on x. The normalized probability distribution for $u_{\parallel} \equiv v_{\parallel}/v_{th}$ in scattering events is found to be

$$f(u_{\parallel}) = \frac{a}{\pi H(a,x)} \frac{e^{-u_{\parallel}^2}}{(x-u_{\parallel})^2 + a^2}. \tag{5.27}$$

Eq.(5.27) is not analytically integrable, so to draw values from this probability distribution we make use of the *rejection method*. Following Zheng and Miralda-Escudé (2002), this is done as follows. We need a random number u from

$$f(u) \propto \frac{e^{-u^2}}{(x-u)^2 + a^2}, \tag{5.28}$$

so we choose as a comparison function

$$g(u) \propto \frac{1}{(x-u)^2 + a^2}. \tag{5.29}$$

A first random number u is chosen from $g(u)$, and then we keep it if a second random number ξ_1 is smaller than e^{-u^2}. Unfortunately, when $x \gg 1$, the chance of acceptance becomes very small. To increase this fraction, the comparison distribution is modified to be

$$g(u) \propto \begin{cases} [(x-u)^2 + a^2]^{-1}\,, & u \le u_0 \\ e^{-u_0^2}[(x-u)^2 + a^2]^{-1}\,, & u > u_0. \end{cases} \tag{5.30}$$

The value of u_0 is chosen as a function of x to minimize the fraction of generated values that will be discarded, and will be discussed next. The acceptance fractions now are e^{-u^2} and $e^{-u^2}/e^{-u_0^2}$ in the regions $u \le u_0$ and $u > u_0$ respectively. Once u_0 is known, we must choose which region to use. To do this a random number ξ is compared to p, defined as

$$p = \frac{\displaystyle\int_{-\infty}^{u_0} g(u)\,du}{\displaystyle\int_{-\infty}^{+\infty} g(u)\,du} \tag{5.31}$$

$$= \left(\theta_0 + \frac{\pi}{2}\right)\left[(1-e^{-u_0^2})\theta_0 + (1+e^{-u_0^2})\frac{\pi}{2}\right]^{-1}, \tag{5.32}$$

where

$$\theta_0 = \tan^{-1}\frac{u_0 - x}{a}. \tag{5.33}$$

u is generated from $u = a\tan\theta + x$, where θ is a random number distributed between $[-\pi/2, \theta_0]$ and $[\theta_0, \pi/2]$ for $R \leq p$ and $R > p$ respectively. Then, another random number ξ determines whether the generated value of u is accepted by comparing it with the corresponding fraction of acceptance.

Following Laursen et al. (2009a), a value of u_0 valid for a wide range of temperatures and frequencies with an acceptance-to-rejection ratio of order unity is achieved when

$$u_0 = \begin{cases} 0 & \text{for } 0 \leq x < 0.2 \\ x - 0.01a^{1/6}e^{1.2x} & \text{for } 0.2 \leq x < x_{\rm cw}(a) \\ 4.5 & \text{for } x \geq x_{\rm cw}(a). \end{cases} \tag{5.34}$$

Here $x_{\rm cw}$ defines the boundary between the core and the wings of the Voigt profile, i.e., where

$$\frac{e^{-x^2}}{\sqrt{\pi}} = \frac{a}{\pi x^2}. \tag{5.35}$$

The solution to this equation can be approximated by

$$x_{\rm cw}(a) = 1.59 - 0.60\log a - 0.03\log^2 a. \tag{5.36}$$

The two velocity components perpendicular to $\boldsymbol{n_i}$, $u_{\perp 1,2}$ are drawn from a Gaussian distribution with zero mean and standard deviation $2^{-1/2}v_{th}$. Following Dijkstra et al. (2006), these components are calculated using the Box-Muller method (see Press et al., 1992) in the following way

$$u_{\perp 1} = \sqrt{-\ln(\xi_1)}\cos(2\pi\xi_2) \tag{5.37}$$

$$u_{\perp 2} = \sqrt{-\ln(\xi_1)}\sin(2\pi\xi_2), \tag{5.38}$$

where both velocities are in units of v_{th}.

Figure 5.1 shows a comparison between the probability distribution of Eq. (5.27) and the numerical algorithm described here for 100,000 values of $u_{\parallel}$. The method reproduces the expected distribution remarkably well, even at the resonance peaks shown.

We will assume that in the frame of the atom, the frequency of the outgoing photon is the same as the incident frequency. In reality, it will differ slightly due to the *recoil effect*, which

accounts for the transfer of small amounts of momentum from the photon to the atom during the scattering process. The average fractional amount of energy transferred per scattering can be written as (Field, 1959)

$$g = \frac{h\Delta\nu_D}{2kT} \tag{5.39}$$

$$= 2.6\times10^{-4}(13\mathrm{kms}^{-1}/v_{th}), \tag{5.40}$$

where h is the Planck constant. For the applications studied in this thesis, the recoil effect has been proven to be negligible (see also the discussion by Adams, 1971).

The new direction $\boldsymbol{n_o}$ is given by a dipole distribution, with the symmetry axis defined by the incident direction $\boldsymbol{n_i}$

$$P(\theta) = \frac{3}{8}(1+\cos^2\theta), \tag{5.41}$$

where θ is the polar angle to the direction $\boldsymbol{n_i}$. The azimuthal angle of the outgoing photon is random and uniform in $0 \leq \phi < 2\pi$.

Finally, the new frequency x' of the photon is given by

$$x' = x - \boldsymbol{n_i}\cdot\boldsymbol{u} + \boldsymbol{n_o}\cdot\boldsymbol{u} \tag{5.42}$$

$$= x - u_{\parallel} + \boldsymbol{n_o}\cdot\boldsymbol{u} \tag{5.43}$$

5.3.5 The resonant scattering calculation in detail

Once the total velocity of the atom is chosen according to the above probability distributions, we first perform a Lorentz transform of the direction and frequency of the photon to the rest frame of the atom. The direction and frequency of the scattered photon are then transformed back to the laboratory frame. Below we will set out how this is done.

The photon's initial direction is

$$\hat{\boldsymbol{n}}_{\boldsymbol{i}} = \sin\theta\cos\phi\,\hat{\imath} + \sin\theta\sin\phi\,\hat{\jmath} + \cos\theta\hat{k}, \tag{5.44}$$

where $\hat{\imath}, \hat{\jmath}$ and $\hat{k}$ are fixed in the lab frame. The atom's velocity satisfies

$$\hat{\boldsymbol{n}}_{\boldsymbol{i}}\cdot\boldsymbol{u} = u_{\parallel} = u\cos\alpha, \tag{5.45}$$

where α is the angle between the direction of the photon and the atom. To calculate α we need to know u, which satisfies

$$u^2 = u_{\parallel}^2 + u_{\perp,1}^2 + u_{\perp,2}^2. \tag{5.46}$$

Note here that u is the velocity of the atom in units of the thermal velocity, v_{th}, Eq. (5.2). In other words,

$$u = \frac{v}{v_{th}}, \tag{5.47}$$

where v[km s^{-1}].

We must now define $\boldsymbol{u}$ in the coordinate system $\{\hat{\boldsymbol{\imath}}, \hat{\boldsymbol{\jmath}}, \hat{\boldsymbol{k}}\}$. At this point $\boldsymbol{u}$ could be pointing in any direction within the cone formed by an angle α from $\hat{\boldsymbol{n}}_i$. To fully specify the atom's direction, we define a set of vectors in the plane perpendicular to $\hat{\boldsymbol{n}}_i$:

$$\boldsymbol{u} = u_{\parallel}\hat{\boldsymbol{n}}_i + u_{\perp,1}\hat{\boldsymbol{n}}_{\perp,1} + u_{\perp,2}\hat{\boldsymbol{n}}_{\perp,2} \tag{5.48}$$

We fix their direction as

$$\hat{\boldsymbol{n}}_{\perp,1} = \sin\phi\hat{\boldsymbol{\imath}} - \cos\phi\hat{\boldsymbol{\jmath}}, \tag{5.49}$$

$$\hat{\boldsymbol{n}}_{\perp,2} = \cos\phi\cos\theta\hat{\boldsymbol{\imath}} + \sin\phi\cos\theta\hat{\boldsymbol{\jmath}} - \sin\theta\hat{\boldsymbol{k}}. \tag{5.50}$$

We can now express $\hat{\boldsymbol{u}}$ as

$$\begin{aligned}\hat{\boldsymbol{u}} &= \frac{1}{u}\Big\{\Big[u_{\parallel}\sin\theta\cos\phi + u_{\perp,1}\sin\phi + u_{\perp,2}\cos\phi\cos\theta\Big]\hat{\boldsymbol{\imath}} \\ &\quad + \Big[u_{\parallel}\sin\theta\sin\phi - u_{\perp,1}\cos\phi + u_{\perp,2}\sin\phi\cos\theta\Big]\hat{\boldsymbol{\jmath}} \\ &\quad + \Big[u_{\parallel}\cos\theta - u_{\perp,2}\sin\theta\Big]\Big\}\hat{\boldsymbol{k}} \\ &\equiv u_i\hat{\boldsymbol{\imath}} + u_j\hat{\boldsymbol{\jmath}} + u_k\hat{\boldsymbol{k}}\end{aligned} \tag{5.51}$$

Since we will perform a Lorentz transformation, we also need to know the coordinates of the vector perpendicular to the velocity of the atom, $\hat{\boldsymbol{u}}_\perp$ lying in the plane formed by $\hat{\boldsymbol{n}}_i$ and $\hat{\boldsymbol{u}}$, which can be defined in the following way:

$$\hat{\boldsymbol{n}}_i = \cos\alpha\hat{\boldsymbol{u}} + (1-\cos^2\alpha)^{1/2}\hat{\boldsymbol{u}}_\perp \tag{5.52}$$

Solving for $\hat{\boldsymbol{u}}_\perp$ we find

$$\begin{aligned}\hat{\boldsymbol{u}}_\perp &= \frac{1}{(1-\cos^2\alpha)^{1/2}}[(\sin\theta\cos\phi - \cos\alpha u_i)\hat{\boldsymbol{\imath}} \\ &\quad +(\sin\theta\sin\phi - \cos\alpha u_j)\hat{\boldsymbol{\jmath}} \\ &\quad +(\cos\theta - \cos\alpha u_k)\hat{\boldsymbol{k}}] \\ &\equiv u_{\perp,i}\hat{\boldsymbol{\imath}} + u_{\perp,j}\hat{\boldsymbol{\jmath}} + u_{\perp,k}\hat{\boldsymbol{k}}.\end{aligned} \tag{5.53}$$

Finally, to perform the Lorentz transformation we need to know the photon's velocity in the directions parallel and perpendicular to the atom's velocity. These are simply

$$n_{i,\parallel}(a) = c\cos\alpha, \tag{5.54}$$

$$n_{i,\perp}(a) = c\sin\alpha. \tag{5.55}$$

So, in the atom's frame, the velocity components of the photon are

$$n'_{i,\parallel}(a) = \frac{c\cos\alpha - v}{1+(v\cos\alpha)/c}, \tag{5.56}$$

$$n'_{i,\perp}(a) = \frac{c\sin\alpha}{\gamma(1+(v\cos\alpha)/c)}, \tag{5.57}$$

where

$$\gamma = \left[1-\left(\frac{v}{c}\right)^2\right]^{-1/2} \tag{5.58}$$

$$\approx 1, \tag{5.59}$$

since $v \ll c$. The above equations can be rewritten as

$$n'_{i,\parallel}(a) = \frac{c\cos\alpha - v_{th}u}{1+u_\parallel v_{th}/c}, \tag{5.60}$$

$$n'_{i,\perp}(a) = \frac{c\sin\alpha}{(1+u_\parallel v_{th}/c)}. \tag{5.61}$$

Now the outgoing photon's direction, $\hat{\boldsymbol{n}}'_o$, satisfies

$$\hat{\boldsymbol{n}}'_{\boldsymbol{o}}\cdot\hat{\boldsymbol{n}}'_{\boldsymbol{i}} = \mu, \tag{5.62}$$

$$\hat{\boldsymbol{n}}'_{\boldsymbol{o}} = \mu\hat{\boldsymbol{n}}'_{\boldsymbol{i}} + \sqrt{(1-\mu^2)}\hat{\boldsymbol{n}}'_{\boldsymbol{i,p}}, \tag{5.63}$$

where $\mu = \cos\theta$, and θ is the polar angle off the initial photon's direction, taken from the dipolar distribution, Eq.(5.41), and $\hat{\boldsymbol{n}}'_{\boldsymbol{i,p}}$ is an arbitrary unit vector perpendicular to $\hat{\boldsymbol{n}}'_{\boldsymbol{i}}$.

Since the scattering is isotropic in the azimuthal angle, its direction must be randomly drawn. The plane formed by the directions parallel and perpendicular to the atom's velocity contains one possible choice for this vector, which we will call $\hat{\boldsymbol{\zeta}}$. In addition, we will call χ the cosine of the angle between $\hat{\boldsymbol{n}}'_{\boldsymbol{i,p}}$ and $\hat{\boldsymbol{\zeta}}$. In other words, if

$$\hat{\boldsymbol{n}}'_{\boldsymbol{i}} = n'_{i,\parallel}(a)\hat{\boldsymbol{a}} + n'_{i,\perp}(a)\hat{\boldsymbol{b}}, \tag{5.64}$$

$$\hat{\boldsymbol{\zeta}} = n'_{i,\perp}(a)\hat{\boldsymbol{a}} - n'_{i,\parallel}(a)\hat{\boldsymbol{b}}, \tag{5.65}$$

where $\{\hat{\boldsymbol{a}}, \hat{\boldsymbol{b}}, \hat{\boldsymbol{c}}\}$ is a set of orthogonal, unit vectors, parallel and perpendicular to the atom's velocity (in fact $\hat{\boldsymbol{a}} \equiv \hat{\boldsymbol{u}}$ and $\hat{\boldsymbol{b}} \equiv \hat{\boldsymbol{u}}_\perp$), then $\hat{\boldsymbol{n}}'_{i,p}$ must satisfy

$$\hat{\boldsymbol{n}}'_{i,p} \cdot \hat{\boldsymbol{\zeta}} = \chi, \tag{5.66}$$

$$\hat{\boldsymbol{n}}'_{i} \cdot \hat{\boldsymbol{n}}'_{i,p} = 0, \tag{5.67}$$

If $\hat{\boldsymbol{n}}'_{i,p} = (p_1, p_2, p_3)$, then the above equations (plus the normalization condition) give

$$n'_{i,\perp}(a)p_1 - n'_{i,\parallel}(a)p_2 = \chi, \tag{5.68}$$

$$n'_{i,\parallel}(a)p_1 = -n'_{i,\perp}(a)p_2, \tag{5.69}$$

$$p_1^2 + p_2^2 + p_3^2 = 1. \tag{5.70}$$

Solving we find

$$\hat{\boldsymbol{n}}'_{i,p} = \frac{n'_{i,\perp}(a)\chi}{c}\hat{\boldsymbol{a}} - \frac{n'_{i,\parallel}(a)\chi}{c}\hat{\boldsymbol{b}} + \sqrt{1-\chi^2}\hat{\boldsymbol{c}}. \tag{5.71}$$

where $\hat{\boldsymbol{c}} \equiv \hat{\boldsymbol{a}} \times \hat{\boldsymbol{b}}$. Now $\hat{\boldsymbol{n}}'_o$ can be written in the basis $\{\hat{\boldsymbol{a}}, \hat{\boldsymbol{b}}, \hat{\boldsymbol{c}}\}$ as

$$\begin{aligned} \hat{\boldsymbol{n}}'_o &= \frac{1}{c}\left(\mu n'_{i,\parallel}(a) + \sqrt{1-\mu^2}\frac{n'_{i,\perp}(a)}{c^2}\chi\right)\hat{\boldsymbol{a}} \\ &\quad + \frac{1}{c}\left(\mu n'_{i,\perp}(a) - \sqrt{1-\mu^2}\frac{n'_{i,\parallel}(a)}{c^2}\chi\right)\hat{\boldsymbol{b}} \\ &\quad + \left(\sqrt{(1-\chi^2}\sqrt{1-\mu^2}\right)\hat{\boldsymbol{c}}, \end{aligned} \tag{5.72}$$

$$\equiv n_{o1}\hat{\boldsymbol{a}} + n_{o2}\hat{\boldsymbol{b}} + n_{o3}\hat{\boldsymbol{c}}. \tag{5.73}$$

In the atom's frame, the photon has also changed its frequency due to the Doppler shift. The frequency seen by the atom corresponds to

$$\nu' = \nu_{\rm em}\gamma\left(1 - \frac{\boldsymbol{v}\cdot\hat{\boldsymbol{n}}_i}{c}\right), \tag{5.74}$$

$$\approx \nu_{\rm em}\left(1 - \frac{v_\parallel}{c}\right), \tag{5.75}$$

where ν' is the frequency seen by the atom and $\nu_{\rm em}$ is the frequency in the laboratory frame.

Now we need to perform a Lorentz transformation back to the laboratory frame. To do this we need to know $n'_{o,\parallel}$ and $n'_{o,\perp}$. Since $\hat{\boldsymbol{a}}$ is the unit vector along the direction of the atom, and $\{\hat{\boldsymbol{b}}, \hat{\boldsymbol{c}}\}$ are perpendicular to it, we can write

$$n'_{o,\parallel} = n_{o1} \tag{5.76}$$

$$n'_{o,\perp} = \sqrt{n_{o2}^2 + n_{o3}^2}. \tag{5.77}$$

The Lorentz transformation is then written as

$$n_{o,\parallel} = \frac{cn'_{o,\parallel} + v_{th}\nu}{1 + \dfrac{v_{th}\nu n'_{o,\parallel}}{c}}, \tag{5.78}$$

$$n_{o,\perp} = \frac{cn'_{o,\perp}}{1 + \dfrac{v_{th}\nu n'_{o,\parallel}}{c}}. \tag{5.79}$$

Now that we are back in the laboratory frame, it is possible to express n_o in terms of the unit vectors parallel and perpendicular to the atom's velocity:

$$\hat{\boldsymbol{n}}_{\boldsymbol{o}} = \frac{1}{c}\left(n_{o,\parallel}\hat{\boldsymbol{u}} + n_{o,\perp}\hat{\boldsymbol{u}}_{\perp,o}\right). \tag{5.80}$$

Since now $\hat{\boldsymbol{n}}_0$ lies on a different plane, $\hat{\boldsymbol{u}}_{\perp,o} \neq \hat{\boldsymbol{u}}_{\perp}$. However, $\hat{\boldsymbol{u}}_{\perp,o}$ is easy to read:

$$\hat{\boldsymbol{v}}_{\perp,o} = \frac{1}{(n_{o2}^2 + n_{o3}^2)^{1/2}}[n_{o2}\hat{\boldsymbol{b}} + n_{o3}\hat{\boldsymbol{c}}]. \tag{5.81}$$

So the only remaining task is to express $\hat{\boldsymbol{c}}$ in the basis $\hat{\imath}, \hat{\jmath}, \hat{k}$. Since $\hat{\boldsymbol{c}} = \hat{\boldsymbol{a}} \times \hat{\boldsymbol{b}}$ we get

$$\hat{\boldsymbol{c}} = (u_j u_{\perp,k} - u_k u_{\perp,j})\hat{\boldsymbol{\imath}} - (u_i u_{\perp,k} - u_k u_{\perp,i})\hat{\boldsymbol{\jmath}} + (u_i u_{\perp,j} - u_j u_{\perp,i})\hat{\boldsymbol{k}}. \tag{5.82}$$

Now it is possible to write

$$\begin{aligned} \hat{\boldsymbol{u}}_{\perp,o} &= \frac{1}{(n_{o2}^2 + n_{o3}^2)^{1/2}}\Big\{[n_{o2}v_{\perp,i} + n_{o3}(u_{\perp,k}u_j - u_k u_{\perp,j})]\hat{\boldsymbol{\imath}} \\ &\quad + [n_{o2}u_{\perp,j} - n_{o3}(u_i u_{\perp,k} - u_k u_{\perp,i})]\hat{\boldsymbol{\jmath}} \\ &\quad + [n_{o2}u_{\perp,k} + n_{o3}(u_i u_{\perp,j} - u_j u_{\perp,i})]\hat{\boldsymbol{k}}\Big\} \\ &\equiv u_{\perp,oi}\hat{\boldsymbol{\imath}} + u_{\perp,oj}\hat{\boldsymbol{\jmath}} + u_{\perp,ok}\hat{\boldsymbol{k}} \end{aligned} \tag{5.83}$$

So finally the outgoing direction of the photon can be written as

$$\hat{\boldsymbol{n}}_o = \frac{1}{c}[(n_{o,\parallel}u_i + n_{o,\perp}u_{\perp,oi})\hat{\boldsymbol{\imath}} + (n_{o,\parallel}u_j + n_{o,\perp}u_{\perp,oj})\hat{\boldsymbol{\jmath}} + (n_{o,\parallel}u_k + n_{o,\perp}u_{\perp,ok})\hat{\boldsymbol{k}}] \tag{5.84}$$

This gives the final direction of the photon, which replaces $\hat{\boldsymbol{n}}_i$ in Eq. (5.44). The frequency shift, is easy to calculate:

$$\nu_f = \nu'\left(1 + \frac{\nu \cdot \hat{\boldsymbol{n}}_{\boldsymbol{o}}}{c}\right), \tag{5.85}$$

$$= \nu_{\rm em}\left(1 - \frac{v_\parallel}{c}\right)\left(1 + \frac{\nu \cdot \hat{\boldsymbol{n}}_{\boldsymbol{o}}}{c}\right) \tag{5.86}$$

Now, for convenience, we express ν in terms of x, defined in Eq.(5.1):

$$\begin{aligned} x_f &= \frac{\nu_{em}}{\Delta\nu_D}\left(1-\frac{v_\parallel}{c}\right)\left(1+\frac{\nu\cdot\hat{\boldsymbol{n}}_{\boldsymbol{o}}}{c}\right)-\nu_0, && (5.87)\\ &= x_i+\frac{\nu_{em}}{\Delta\nu_D}\left(\frac{\nu\cdot\hat{\boldsymbol{n}}_{\boldsymbol{o}}}{c}-\frac{v_\parallel}{c}\right), && (5.88)\\ &= x_i+\frac{\nu_{em}}{\nu_0}\left(\frac{\nu\cdot\hat{\boldsymbol{n}}_{\boldsymbol{o}}}{v_{th}}-\frac{v_\parallel}{v_{th}}\right), && (5.89)\\ &= x_i+\frac{\nu_{em}}{\nu_0}(u\cdot\hat{\boldsymbol{n}}_{\boldsymbol{0}}-u_\parallel) && (5.90)\end{aligned}$$

Usually $\nu_{em}\approx\nu_0$, in which case the expression reduces to what we already had in Eq.(5.43).

Finally, the dot product $\boldsymbol{u}\cdot\hat{\boldsymbol{n}}_{\boldsymbol{o}}$ is equal to

$$\boldsymbol{u}\cdot\hat{\boldsymbol{n}}_o=\frac{u}{c}[u_i(n_{o,\parallel}u_i+n_{o,\perp}u_{\perp,oi})+u_j(n_{o,\parallel}u_j+n_{o,\perp}u_{\perp,oj})+u_k(n_{o,\parallel}u_k+n_{o,\perp}u_{\perp,ok})] \quad (5.91)$$

5.3.6 Accelerating the code

The algorithm described above will follow the scattering events of a photon until it escapes (or is absorbed), and then the process starts again with a new photon travelling on a different path, and so on until we are satisfied with the number of photons generated. In practise, for the runs shown in this thesis the number of photons generated varies between a few thousand up to several hundred thousand, depending on the accuracy of the result we wish to achieve.

For the typical HI regions studied here, the number of scatterings that photons will undergo before escaping could be as high as several tens or hundreds of millions. If we want to model several thousand photons, then the total number of calculations grows enormously and the task could become computationally infeasible. However, most of the scattering events will occur when the photon is at the line centre, or very close to it, where the cross section for scattering peaks. Eq.(5.16) shows that the cross section for scatterings reduces as $\sim e^{-x^2}$ near the line centre, and as $\sim x^{-2}$ away from it. Whenever the photon falls near the centre it will experience so many scatterings that the actual distance travelled between each scattering event will be negligible, since in this case it will be most likely scattered by an atom with a velocity close to zero (see Fig. 5.1). Hence, the frequency after such scattering will remain in the resonant core. This motivates the possibility for accelerating the code performance by skipping those *inconsequential* scattering events.

Following Dijkstra et al. (2006), a critical frequency x_{crit} defines a transition from the resonant core to the wing. Whenever a photon is in the core (with $x < |x_{crit}|$) we can push it to the wings by allowing the photon to be scattered only by a rapidly moving atom. We do this by modifying the distribution of perpendicular velocities by a *truncated* Gaussian, i.e. a distribution which is a Gaussian for $u > x_{crit}$ but which is zero otherwise. The modified perpendicular velocities are then drawn from

$$u_{\perp 1} = \sqrt{x_{crit}^2 - \ln(\xi_1)}\cos(2\pi\xi_2) \quad (5.92)$$

$$u_{\perp 2} = \sqrt{x_{crit}^2 - \ln(\xi_1)}\sin(2\pi\xi_2). \quad (5.93)$$

When doing this, we allow the photon to redshift or blueshift away from the line centre, thus reducing the cross section for scattering and increasing the path length. For the configurations studied here, we found that a value of $x_{crit} = 3$ provides a good balance between accuracy and efficiency of the code, reducing the execution time by a factor 100 or more with respect to the non-accelerated case.

5.3.7 Output of the code

We allow the code to generate output in two modes:

- A *detailed* output file for each photon, in which its position and frequency is stored for every interaction followed by the code, until the photon either escapes from the HI region or is absorbed by a dust grain. Other properties are also stored, such as the velocity of the atom (if relevant) at the moment of scattering, and the running time until each interaction event. This output mode is obviously inefficient when studying a large set of photons, so it is used mainly for debugging purposes.

- A *short* output file, which stores the frequency and position of all photons at the moment they either escape or are absorbed by dust, along with other properties such as the time it took the code to compute each escape/destruction of photons. This is the preferred mode of output to compute quantities which require a large number of photons, such as the emergent spectrum or the escape fraction of photons.

5.4 Validation of the code

The flexibility of this numerical approach allows us to reproduce configurations for which analytical solutions are available. Hence, these analytical solutions are ideal to test the performance of the code. In the following we will describe the tests we have performed on our code, which prove its accuracy. Each comparison with an analytical solution is meant to test a different aspect of the code, which is why a proper validation requires to test the code against several analytical solutions.

5.4.1 The redistribution function

Hummer (1962) (and later on Lee, 1974) computed the redistribution in frequency of radiation scattered from moving atoms. Both authors studied several cases including coherent and non coherent scattering with isotropic or dipolar angular distributions and absorption profiles with zero natural line widths or Voigt profiles. In our case, we are interested in the redistribution function arising from coherent scattering in the rest frame of the atom, with a dipolar angular distribution and including radiation damping. The expression for the redistribution function is

$$R_{II-B}(x,x') = \frac{3\pi^{-3/2}}{8} a \int_{|\overline{x}-\underline{x}|/2}^{\infty} e^{-u^2} \int_{\overline{x}-u}^{\underline{x}+u} \left[3 - \left(\frac{x-t}{u}\right)^2 - \left(\frac{x'-t}{u}\right)^2 + 3\left(\frac{x-t}{u}\right)^2 \left(\frac{x'-t}{u}\right)^2 \right] \frac{\mathrm{d}t\ \mathrm{d}u}{t^2+a^2}, \quad (5.94)$$

where x and x' are the frequency of the photon before and after the scattering and $\overline{x}$ and $\underline{x}$ are the maximum and minimum between $|x|$ and $|x'|$ respectively. This expression cannot be computed analytically (although the integral over t is simple, the resulting expression is too complicated to be shown here), so it must be computed numerically. It is also possible to compute the redistribution function using our Monte Carlo code described above. Figure 5.2 shows the resulting redistribution function for 3 different initial frequencies using $\sim 10^5$ photons, and the remarkably good agreement between the Monte Carlo code and the analytical expression of Eq.(5.94).

Photons at the line centre are more likely to remain in the line centre after a scattering event, since the redistribution function is very narrow and peaks at $x_f = 0$. For a photon with an incoming frequency of $x_i = 5$, there is a non-zero chance to get closer to the line centre.

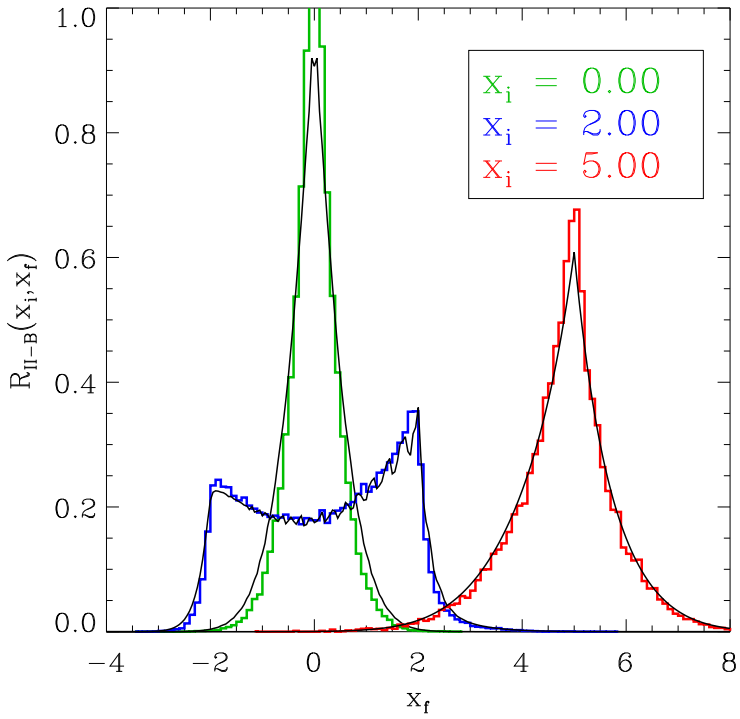

Figure 5.2: The redistribution function of Lyα photons scattered by hydrogen atoms for different initial frequencies. The histograms show the resulting frequency distribution from the Monte Carlo code, whereas the solid curves show a numerical integration of Eq. (5.94).

If this happens, subsequent scattering will increase the probability of approaching the line centre even further, until the photon will eventually reach the line centre. Once there, it is very difficult to change its frequency, which is why most of the scatterings tend to happen in the line centre.

5.4.2 Lyα spectrum from a static slab

The emergent spectrum from an optically thick, homogeneous static slab with photons generated at the line centre was first calculated by Harrington (1973), and the result was generalised by Neufeld (1990), allowing the generated photons to have any frequency. Harrington's solution for the emergent Lyα spectrum for a slab with thickness characterised by its

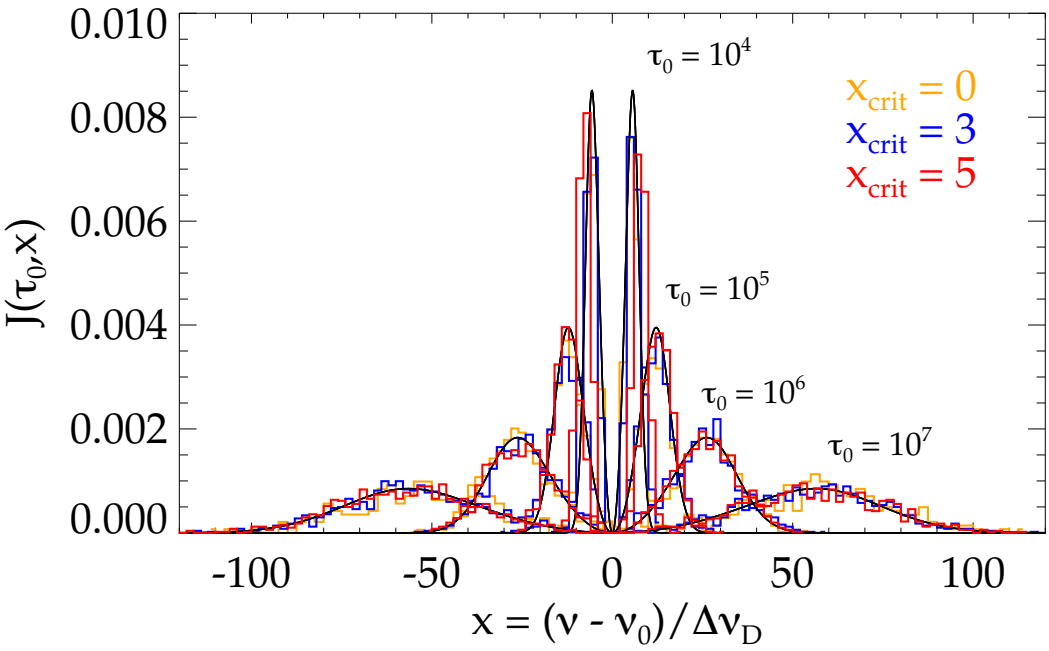

Figure 5.3: Lyα spectrum emerging from a homogeneous static slab at $T = 10$[K], for optical depths at the line centre of $\tau_0 = 10^4, 10^5, 10^6$ and 10^7, as shown in the plot. The profiles are symmetric around $x = 0$. The more optically thick the medium, the farther from the line centre the resulting peaks of each profile are found. The solid lines show Harrington (1973) analytical solution, and the orange, blue and red histograms show the results from the Monte Carlo code for a choice of $x_{crit} = 0, 3$ and 5 respectively.

optical depth at the line centre τ_0, is

$$J(\pm\tau_0, x) = \frac{\sqrt{6}}{24}\frac{x^2}{\sqrt{\pi}a\tau_0}\frac{1}{\cosh\left[\sqrt{\pi^3/54}x^3/(a\tau_0)\right]}. \quad (5.95)$$

The above expression is valid when $a\tau_0 \geqslant 10^3/\sqrt{\pi}$, or for $\tau_0 \geqslant 1.2\times10^6$ when $T = 10^4$K.

Figure 5.3 shows the emergent spectrum from a simulated homogeneous slab. The temperature of the medium was chosen to be $T = 10$K, since in this regime the analytical expression is accurate for optical depths down to $\tau_0 \sim 10^4$, which is faster to compute with the code.

The typical Lyα flux profile is double peaked, and is symmetrical with respect to the line centre. The centre of the peaks is displaced away from $x = 0$ by a value determined by τ_0. The higher the optical depth, the farther away from the line centre and the wider the profile will be. Figure 5.3 compares the analytic solution of Harrington (1973) with the ouput from the basic code (orange histogram), and two accelerated versions of it (blue and red histograms). Overall, it is clear that the non-accelerated version of the code reproduces the analytical formula over the range of optical depths shown here. When $x_{crit} = 3$ (the blue histogram in Fig. 5.3), the output is virtually indistinguishable from the non-accelerated version, but the running time has been decreased by a factor ~ 200. If we increase x_{crit} to 5 then the agreement with the analytical result breaks down at $\tau_0 = 10^4$, shifting the peaks slightly further away from the centre than the correct result. This occurs because some photons were expected to escape with frequencies of $x \leq 5$ at this optical depth, but since $x_{crit} = 5$ those photons were pushed into the wings of the absorption profile. The net effect is a shift in the resulting spectrum.

Figure 5.3 confirms that the choice of $x_{crit} = 3$ does not compromise the accuracy of the results, although larger values do.

5.4.3 Mean number of scatterings

Harrington (1973) also computed the mean number of scatterings expected before a Lyα photon escapes from an optically thick medium for the homogeneous slab. The result, already studied by Avery and House (1968) using a Monte Carlo technique, is

$$\langle N_{scat}\rangle = 1.612\tau_0. \quad (5.96)$$

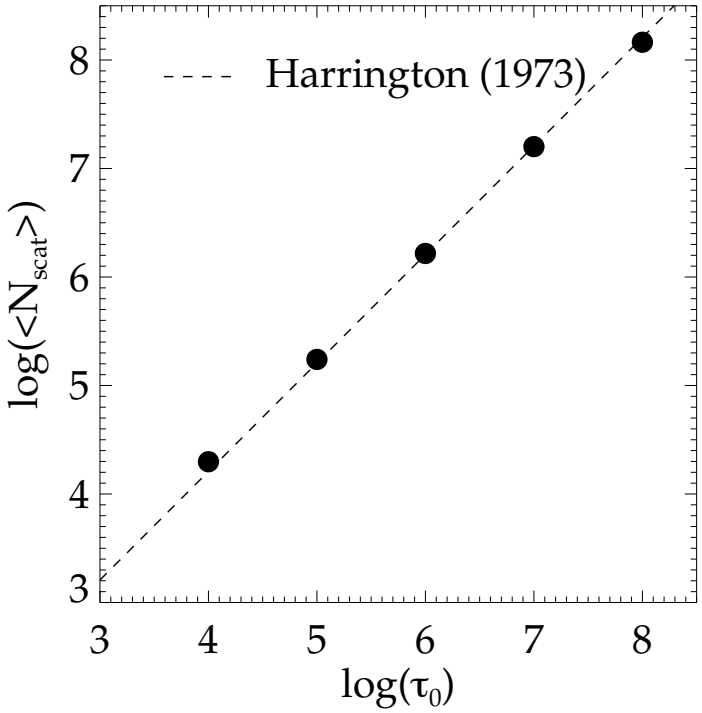

Figure 5.4: Mean number of scatterings as a function of the optical depth in the line centre of the medium. The circles show the results from the Monte Carlo code for configurations with different τ_0. The dashed line shows the analytical solution of Harrington (1973).

Fig. 5.4 shows a comparison between the mean number of scatterings computed using our code against the analytical prediction of Harrington (1973). The agreement is remarkably good.

5.4.4 Lyα spectrum from a static sphere

Following closely the methodology of Harrington (1973) and Neufeld (1990), Dijkstra et al. (2006) computed the emergent spectrum from a static sphere. Their result is

$$J(x,\tau_0) = \frac{\sqrt{\pi}}{\sqrt{24}a\tau_0}\left[\frac{x^2}{1+\cosh\left[\sqrt{2\pi^3/27}(|x^3|/a\tau_0)\right]}\right], \tag{5.97}$$

which looks very similar to the expression for the emergent spectrum from an homogeneous slab, Eq. (5.95). Fig. 5.5 shows a comparison between the analytic prediction and the output from the code at different optical depths. Again, there is a very good agreement between the two. The optical depths shown in Fig.5.5 were chosen to be different from those in Fig.

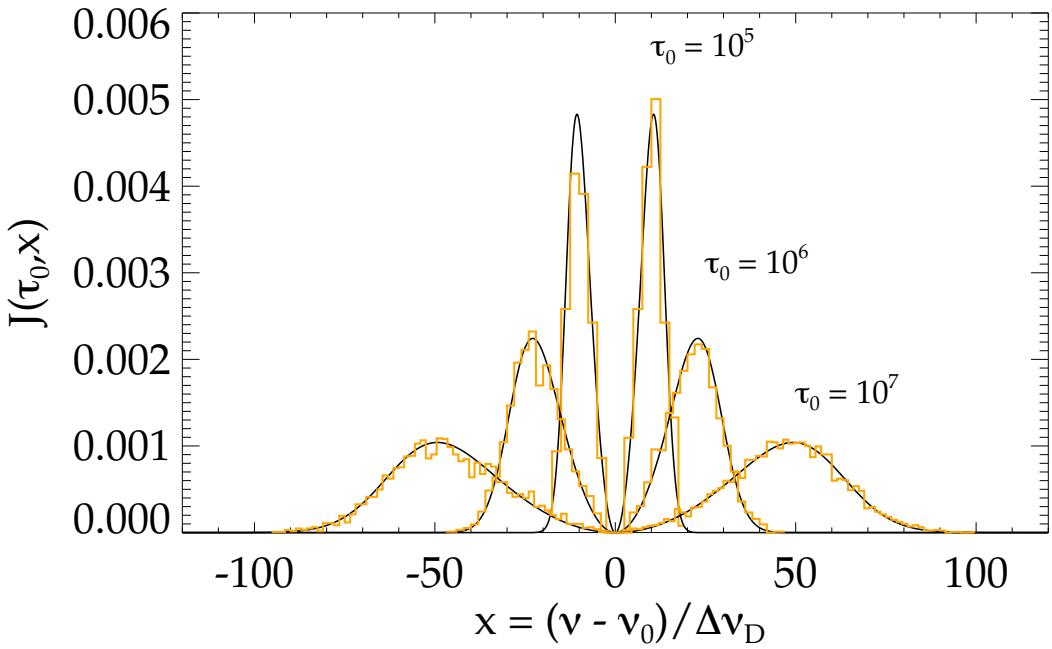

Figure 5.5: Lyα spectrum emerging from a homogeneous static sphere at $T = 10$K, for optical depths at the line centre of $\tau_0 = 10^5, 10^6$ and 10^7. The profiles are symmetric around $x = 0$. The thicker the medium, the farther from the line centre the resulting peaks of each profile are found. The solid lines show the analytical solution of Dijkstra et al. (2006) (Eq. 5.97), and the histograms show the results from the Monte Carlo code.

5.3 to show that the code is following closely the expected emergent spectrum for a range of optical depths spanning several orders of magnitude.

5.4.5 f_{esc} from a static dusty slab

Neufeld (1990) computed an analytical expression for the escape fraction of photons emitted from an homogeneous, dusty slab. The solution, valid for very high optical depths ($a\tau_0 > 10^3$), and in the limit $(a\tau_0)^{1/3} \gg \tau_a$, where τ_a is the optical depth of absorption by dust (Eq. 5.24), is

$$f_{esc} = \frac{1}{\cosh\left[\zeta'\sqrt{(a\tau_0)^{1/3}\tau_a}\right]}, \tag{5.98}$$

where $\zeta' \equiv \sqrt{3}/\zeta\pi^{5/12}$, and $\zeta \approx 0.525$ is a fitting parameter.

Fig. 5.6 shows a comparison between the escape fraction obtained from a series of simula-

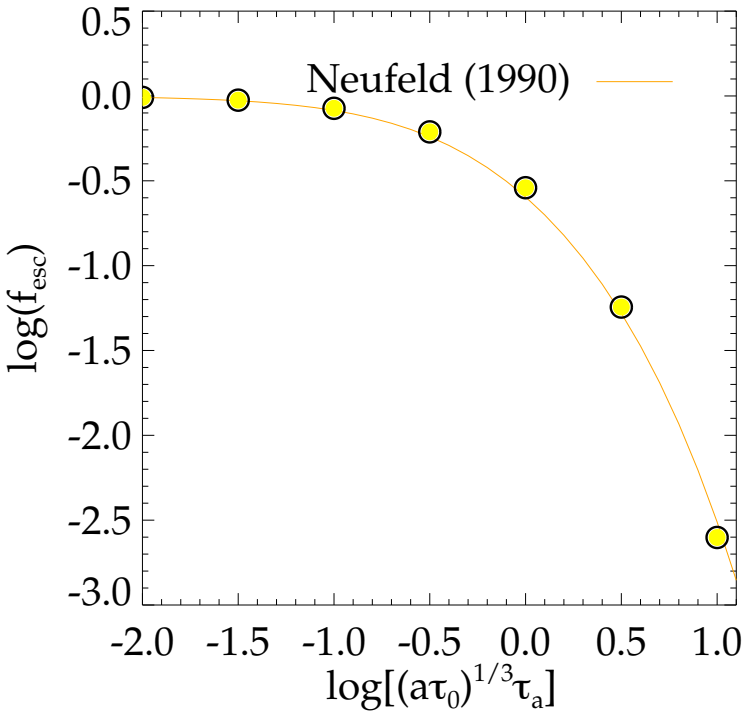

Figure 5.6: The escape fraction of Lyα photons from an homogeneous dusty slab. The optical depth of hydrogen scatterings at the line centre τ_0 is held constant at $\tau_0 = 10^6$, and different values of the optical depth of absorption τ_a are chosen. Circles show the output from the code, and the solid orange curve shows the analytical prediction of Neufeld (1990), Eq. (5.98)

tions, keeping τ_0 fixed and varying τ_a, with the analytical solution of Eq. (5.98). The escape fraction, as expected, decreases rapidly for increasing τ_a, which, for a fixed τ_0, translates into having a higher concentration of dust in the slab. It is worth noting that the escape fraction depends not only on the amount of dust, but also in the temperature of the gas (through the a parameter), the column density of hydrogen (which defines the number of scatterings in the medium, Eq. 5.96) and the amount of dust through τ_a. In a more general case, as we will see next, the mean number of scatterings is also regulated by the bulk motions of the gas, so in practice the escape fraction will depend on the bulk velocity of the gas as well.

5.4.6 Comparison with a similar code: Lyα spectrum from an expanding sphere

Another important parameter yet not taken into account is the bulk velocity of the medium. As will be shown in the next chapter, the velocity of the medium plays a crucial role shaping

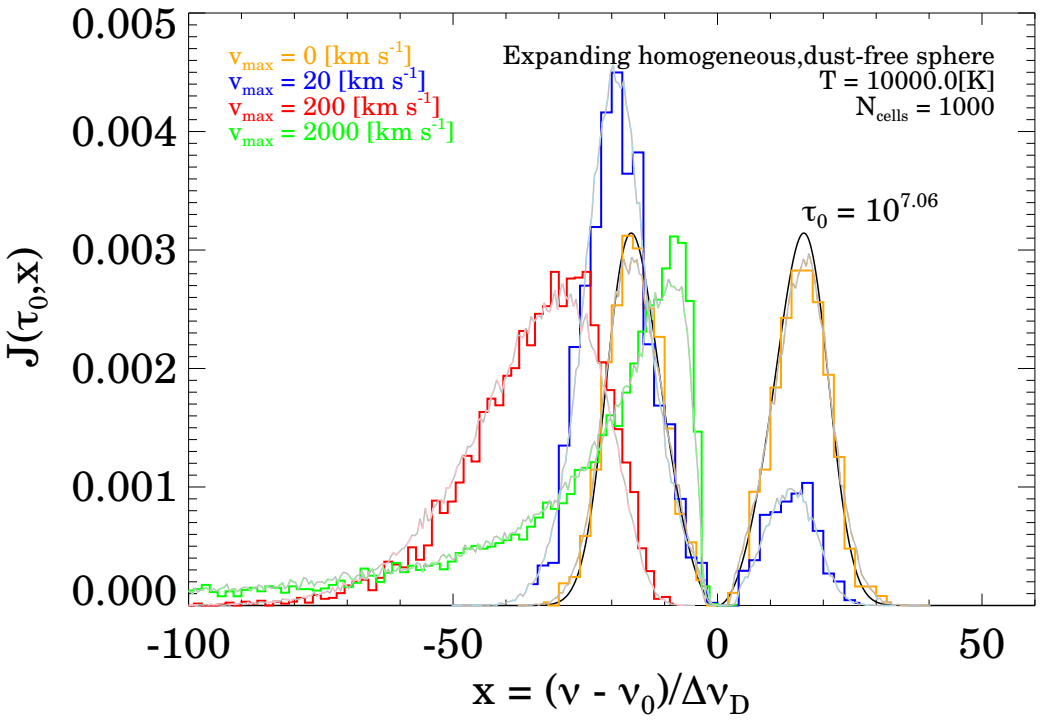

Figure 5.7: The emergent Lyα spectrum from a linearly expanding sphere with velocity zero at the centre and velocity at the edge $v_{max} = 0, 20, 200$ and 2000km/s shown in orange, blue, red and green respectively. The optical depth at the line centre is kept fixed at $\tau_0 = 10^{7.06}$. The analytical solution of Dijkstra et al. (2006) for the static case is shown in black. The coloured histograms show the output from the code. The coloured solid curves show the results obtained with the Laursen et al. (2009a) code (their Fig. 8).

the profile of the emergent spectrum and the escape fraction as well.

To study the effect of bulk motions in the gas, we model the case of an expanding homogeneous sphere, with a velocity at a distance $\boldsymbol{r}$ from the centre given by

$$v_{bulk} = H\boldsymbol{r}, \tag{5.99}$$

$$H = \frac{v_{max}}{R}, \tag{5.100}$$

where v_{max} is the velocity of the sphere at its edge, and R is the radius of the sphere.

There is no analytical solution for this configuration (except when $T = 0$, see Loeb and

Rybicki (1999)), so we decided to compare our results to those found by a similar Monte Carlo code. Fig. 5.7 shows a comparison between our code and the results obtained with the MoCaLaTA Monte Carlo code (Laursen et al., 2009a), kindly provided by Peter Laursen. The agreement between the two codes is encouraging. Moreover, the figure helps us understand the effect of bulk motions of the gas in the emergent spectrum. First, when $v_{max} = 0$ we obviously recover the static solution, Eq. (5.97). When $v_{max} = 20$km/s, the velocity of the medium causes photons to have a higher probability of being scattered by atoms with velocities dominated by the velocity of the medium. These atoms *see* the photons as being redshifted, and hence the peak of the spectrum is shifted slightly towards the red part of the spectrum, although still a fraction of photons appear to escape blueshifted.

When $v_{max} = 200$km/s, the blue peak is completely erased, and the peak is shifted even further to the red side. For very high velocities, such as $v_{max} = 2000$km/s, the velocity gradient makes the medium optically thin, and the average number of scatterings decreases drastically, and consequentially the photons have less chance of being redshifted far into the wings, thus shifting the peak back to the centre, but still with no photons in the blue side of the spectrum.

All the tests described in this section were used to validate our Monte Carlo code, but they also served as an example of the performance and range of possibilities open to study with our code. In the next chapter we will develop a model which will be suitable to be coupled with the output from GALFORM, so that we can assign an escape fraction to each galaxy and study statistical properties of Lyα emitters.